scientific reports

Check for updates

OPEN

Skeletal muscle insulin resistance in prediabetes: a lipidomic perspective on diacylglycerols, ceramides, and phospholipids

Irena Markova[1]✉, Martina Hüttl[1], Jakub Šťastný[2], Iveta Zapletalova[3], Petr Kačer[2], Vladimír Hönig[2], Tereza Kacerova[2,4] & Hana Malinska[1]

Lipid metabolism disorders, accompanied by the accumulation of lipids, are believed to contribute to skeletal muscle insulin resistance development. These alterations may attenuate insulin signaling and glucose uptake and utilization. However, the specific roles of individual lipids remain incompletely understood. The study examined the relationship between skeletal muscle lipid composition and insulin resistance in a non-obese prediabetic hereditary hypertriglyceridemic (HHTg) rats. Male HHTg rats aged 4 and 12 months, exhibiting insulin resistance, and dyslipidaemia were used in this study. Skeletal muscle lipidomic profiles were analyzed using tandem mass spectrometry. Compared to age-matched Wistar controls, HHTg rats exhibited increased serum triglycerides, elevated NEFA and impaired glucose tolerance. Impaired muscle insulin sensitivity in HHTg rats was associated with the accumulation of triglycerides and 1,3-diacylglycerols, and most notably with an increase in specific ceramide species (18:0, 22:0, 24:0, 24:1) in both 4- and 12-month-old animals. Elevated mRNA expression of *Degs1*, a key enzyme in ceramide biosynthesis, may underlie the observed ceramide accumulation. Lipidomic profiling revealed decreases in membrane phospholipids, including phosphatidylethanolamine (PE 41:2), lysophosphatidylcholine (LPC 22:6), and lysophosphatidylethanolamine (LPE 20:0). In HHTg prediabetic model, skeletal muscle insulin resistance develops independently of obesity and prior to diabetes onset, driven by the accumulation of lipotoxic diacylglycerols and ceramides, alongside a reduction in specific phospholipids and lysophospholipids. Impaired fatty acid oxidation and enhanced ceramide biosynthesis contribute to ectopic lipid deposition, with ceramides exerting a more pronounced effect on insulin signaling. Strain-specific alterations in lipid metabolism are more significant than age-related alterations.

Keywords Skeletal muscle, Insulin sensitivity, Lipidomics, Diacylglycerols, Ceramides, Phospholipids

Abbreviations

Acaca	Acetyl-coenzyme A carboxylase alpha
AUC	Area under curve
CERs	Ceramides
Cers1	Ceramide synthase 1
DAGs	Diacylglycerols
Degs1	Delta 4-desaturase sphingolipid 1
FA	Fatty acid
FGF21	Fibroblast growth factor 21
HHTg	Hereditary hypertriglyceridemic
IR	Insulin resistance
IRS1	Insulin receptor substrate 1
LPC	Lysophosphatidylcholine

[1]Centre for Experimental Medicine, Institute for Clinical and Experimental Medicine, Prague, Czech Republic. [2]Faculty of Agrobiology, Food and Natural Resources, Czech University of Life Sciences, Prague, Czech Republic. [3]Department of Pharmacology, Faculty of Medicine and Dentistry, Palacky University Olomouc, Olomouc, Czech Republic. [4]Chemistry Research Laboratory, Department of Chemistry, University of Oxford, Oxford OX1 3TA, UK. ✉email: irma@ikem.cz

LPE	Lysophosphatidylethanolamine
NEFA	Non-esterified fatty acid
PC	Phosphatidylcholine
PCA	Principal component analysis
PKB/Act	Protein kinase B
PKC	Protein kinase C
PE	Phosphatidylethanolamine
PE-O	Phosphoethanolamine
Scd1	Stearoyl-coenzyme A desaturase 1
TGs	Triglycerides
TLR-4	Toll-like receptor 4
T2DM	Type 2 diabetes mellitus

Insulin resistance (IR) is recognized as a central and early feature in the pathogenesis of type 2 diabetes mellitus (T2DM) that can be detected ahead of the β-cell failure and hyperglycaemia and may precede the clinical manifestation of T2DM by 10–20 years[1]. Numerous factors have been implicated in IR development including increased visceral adiposity, aging, dysregulated adipose tissue and lipid metabolism. Impaired lipid metabolism contributes to both the onset and progression of T2DM.

Elevated plasma triglycerides (TGs) and non-esterified fatty acids (NEFAs) are closely associated with decreased insulin sensitivity in human studies[2]. Dyslipidaemia and lipid excess leads to the accumulation of intramyocellular lipid metabolites, which coincides with impaired insulin response. Previous studies have demonstrated that skeletal muscle TG accumulation is associated with IR in various animal models - in obese non-diabetic, diabetic rat model[3] as well in non-obese prediabetic hereditary hypertriglyceridemic (HHTg) rat strain[4]. However, these studies did not assess the presence of lipotoxic metabolites or propose potential underlying mechanisms. Skeletal muscle is responsible for a substantial proportion of lipid mobilisation for oxidative metabolism and accounts for up to 80% of insulin-stimulated whole-body glucose disposal. Consequently, skeletal muscle plays a pivotal role in the development of IR and in the maintenance of glucose homeostasis.

The role for lipids as mediators of IR was proposed early on[5]. Ectopic lipid accumulation in skeletal muscle has been shown to impair insulin signal transduction, induce pro-inflammatory cytokine production and promote oxidative stress. Nevertheless, the specific contribution of individual lipid species remains poorly understood. Findings from previous studies investigating lipid species such as diacylglycerols (DAGs) and ceramides (CERs) have been inconclusive. While DAGs are frequently elevated in skeletal muscle in the context of obesity and T2DM, their association with IR has been demonstrated in some but not all studies[6]. Higher levels of CERs in muscle have been observed in obese and diabetic patients[7]. Although elevated CERs are usually associated with IR, not all CER species are metabolically detrimental.

Complexity of lipid species can be evaluated by completed lipid profile produced in lipidomic analysis. To date, only a limited number of studies have characterised the lipidomic profile of skeletal muscle. A human study in obese, non-diabetic participants[8] identified C18:0 sphingolipids in muscle as potential contributors to IR. Several animal studies investigating the skeletal muscle lipidomic signature have similarly highlighted alterations predominantly in sfingolipids and CERs profiles[9,10]. However, these studies primarily focused on lipidomic differences across various tissues rather than muscle-specific changes. Moreover, all available animal studies were conducted in models of high-fat diet-induced IR, inherently associated with obesity and excessive visceral adiposity.

In this study, we investigated the skeletal muscle lipidomic profile and identified lipid species that potentially may contribute to the development of IR in a non-obese prediabetic model – the HHTg rat. This strain is characterised by genetically determined hypertriglyceridaemia, peripheral tissue IR, impaired glucose tolerance, and hepatic steatosis, all occuring in the absence of obesity[11,12]. We studied two age groups of animals (4- and 12-month-old rats) because aging is an important factor in the development of IR. Lipidomics was monitored in relation to insulin sensitivity parameters and gene expression of key enzymes and transcription factors involved in lipid metabolism.

Methods

Animals and diet

All experiments were performed in agreement with the Animal Protection Law of the Czech Republic (359/2012) and the Directive 2010/63EU of the European Parliament and of the Council and were approved by the Ethics Committee of the Institute for Clinical and Experimental Medicine, Prague (Protocol Number: 35/2022). The study is reported in accordance with ARRIVE guidelines. At the beginning of the study, the animals were randomized into four experimental groups. The study was performed on 4- and 12-month-old male Wistar rats (obtained from Charles River, Germany) as the control group and 4- and 12-month-old male HHTg rats (provided by the Institute for Clinical and Experimental Medicine, Prague, Czech Republic) as the non-obese pre-diabetic model ($n=7$ in each group). Rats were held in cages under temperature- (22 °C) and humidity-controlled conditions under a 12-h/12-h light/dark cycle with free access to food (maintenance diet for rats and mice; Altromin, Germany) and drinking water. At the end of the experiment, rats were killed by decapitation after light anesthesia (Zoletil 5 mg/kg b.wt.) in a postprandial state. Aliquots of serum and tissue samples were collected and stored at -80 °C for further analysis.

Analytical methods/biochemical analyses

Serum levels of TGs, glucose, NEFA, total and HDL cholesterol were measured using commercially available kits (Erba Lachema, Brno, Czech Republic and Roche Diagnostics, Mannheim, Germany). Serum insulin and irisin concentrations were determined using ELISA kits (Rat Insulin Mercodia AB, Sweden and Irisin kit, BioVendor, Czech Republic). Adiponectin as well fibroblast growth factor 21 (FGF21) were determined using the Rat ELISA kits (MyBioSource, USA).

For the oral glucose tolerance test (OGTT), blood glucose was determined after a glucose load (300 mg / 100 g b.wt.) administered intragastrically after overnight fasting. Blood was drawn from the tail before the glucose load at 0 min and then at 30, 60 and 120 min thereafter.

For determination of TGs in skeletal muscles (*musculus gastrocnemius*), tissue samples were powered under liquid N_2 and extracted in chloroform/methanol (2:1), after which 2% KH_2PO_4 was added and the solution was centrifuged. The organic phase was evaporated under N_2 and the resulting pellet was dissolved in isopropyl alcohol, after which TG content was determined by enzymatic assay (Erba-Lachema, Czech Republic). To determine DAGs in the muscle (*musculus gastrocnemius*), samples were extracted in dichloromethane/methanol followed by the addition of 2% KH_2PO_4. After centrifugation, the organic phase was evaporated under N_2 and the resulting pellet was dissolved in isopropyl alcohol and isolated by thin-layer chromatography using hexane/diethylether/acetic acid (70:30:1) as a solvent. The content of separated DAGs was extracted from silica gel and quantified by enzymatic assay (Erba-Lachema, Czech Republic).

Basal and insulin-stimulated glycogen synthesis as markers of skeletal muscle insulin sensitivity were determined ex vivo in isolated *musculus soleus* by measuring the incorporation of ^{14}C-U glucose into glycogen, as described previously[13]. Glucose and palmitate oxidation in muscle were measured ex vivo in isolated *musculus soleus* based on incorporation of radiolabeled substrates ^{14}C-U glucose and ^{14}C-palmitate into CO_2, as described previously[13].

Western blot analysis of protein kinase C (PKC)

Muscle tissue (*musculus gastrocnemius*) was homogenized and utilized to obtain cytosolic and membrane fraction as described previously[14,15]. Briefly, muscle samples were homogenized in Tris-HCl buffer supplemented with protease inhibitors and centrifuged at 105,000 g for 60 min. The supernatant represented the cytosolic fraction, the sediment representing membrane fraction was resuspended in homogenization buffer and then centrifuged for further 60 min. Aliquots of both fractions were used for Western blot analyses. Protein content was determined according to Lowry assay modified by Peterson[16].

Samples were subjected to sodium dodecylsulphate polyacrylamide gel electrophoresis, than transferred to a nitrocellulose membrane. After the blocking step (5% dry low-fat milk in TTBS buffer (Tris-buffered saline with Tween 20: 0.02 M Tris, 0.5 M NaCl, 0.1% Tween 20, pH 7.5)), membranes were washed in TTBS buffer and probed with PKCε and PKCθ isoform-specific primary rabbit antiserum (PKCε: 1:8,000 in TTBS, SAB5702995, Sigma, Saint Luis, MO, USA; PKCθ: 1:1,500 in TTBS, sc-212, Santa Cruz Biotechnology, Santa Cruz, CA, USA,). After washing step, membranes were incubated with the secondary swine anti-rabbit IgG antibody labeled with horseradish peroxidase (1:4,000 in TTBS, Swar/Px, Sevapharma, Prague, Czech Republic). To ensure the specificity of PKCε- and PKCθ-immunoreactive proteins, prestained molecular weight protein standards (Fluka) and the respective blocking immunizing peptides were used. β-actin was used as an internal reference. Immunoreactive proteins were made visible using chemiluminiscence reagents (Amersham Int., Aurora, Ohio, USA) and exposure to autoradiographic film. For the quantification of the relative abundance of PKC isoforms scanning and Quantity One software (Bio-Rad, Hercules, CA, USA) were used.

Relative mRNA expression

Total RNA was isolated from muscle tissue (*musculus gastrocnemius*) using RNA Blue (Top-bio, Vestec, Czech Republic). The purity and concentration of RNA was measured using Nanodrop One (Thermo Fisher Scientific, MA, USA). Reverse transcription was performed with EvoScript Universal cDNA Master kit (Roche, Basel, Switzerland) using Mastercycler Epgradient S instrument (Eppendorf, Hamburg, Germany). The quantitative real-time PCR was performed on 1536-well format plates using acoustic liquid handler Echo 550 (Labcyte, Dublin, Ireland) and LightCycler 1536 Instrument (Roche, Basel, Switzerland). TaqMan Gene Expression Assays (Thermo Fisher Scientific, MA, USA) were used to determine individual genes. Relative expressions were determined after normalization against *Hprt1* as an internal reference and calculated using the $2^{-\Delta\Delta Ct}$ method.

Pseudotargeted lipidomics analysis

Lipid extraction from muscle tissue (*musculus gastrocnemius*) was carried out using a modified Folch method optimized for pseudotargeted lipidomics. Deep-frozen tissue was cryogenically pulverised to obtain a homogeneous powder. Each sample was extracted with ice-cold methanol, followed by chloroform (1:2 v/v). After incubation, ice-cold water was added to achieve a final chloroform: methanol: water ratio of 8:4:3 (v/v/v), followed by a further incubation. Phase separation was achieved by centrifugation (8,000 rpm, 5 min, 4 °C). The organic layer was collected, and the aqueous phase was re-extracted to maximize lipid recovery. Combined organic phases were dried under nitrogen. Prior to analysis, lipids were reconstituted in acetonitrile: isopropanol: water (65:30:5, v/v/v).

Lipidomic profiling was performed using an Ultimate 3000 HPLC system (Dionex, Sunnyvale, CA, USA) equipped with a C18 column (100 Å, 3.5 µm, 2.1 × 150 mm; Waters, Milford, MA, USA), coupled to a TripleTOF mass spectrometer 5600 + with an ESI source (AB Sciex, Toronto, Canada). Data were acquired in Multiple Reaction Monitoring–High Resolution (MRMHR) mode following the AB Sciex QTOF-MS standard workflow[17].

Raw data were pre-processed prior to statistical analysis. Features with values below the limit of quantification (LOQ) were excluded, and remaining missing values were imputed as 20% of the minimum positive value for

each variable. The resulting dataset, which contained < 1% missing values, was median normalized, Pareto scaled, and log-transformed to reduce heteroscedasticity and improve comparability across samples.

A Pearson correlation analysis was performed in R (*corrplot* package) to assess linear relationships between skeletal muscle lipid species and metabolic parameters. Correlation coefficients (*r*) were visualised in a correlation matrix.

Statistical analysis

Two-way ANOVA was used to analyse the individual and combined effects of treatment and strain for treatment-vs.-strain interactions. All data analysed were of normal distribution. Fisher's LSD *post-hoc* test was used for variables showing evidence of treatment-vs.-strain interactions. The test was adjusted for multiple comparisons to determine strain and age effect in HHTg and Wistar strains. Statistical significance was determined at a value of $p < 0.05$. All results are expressed as mean ± SEM. Statistical analysis was performed using StatSoft Statistica 14 (StatSoft CZ; Czech Republic).

Multivariate analysis for targeted lipidomics was performed using both unsupervised and supervised approaches in MetaboAnalyst 6.0[18]. Principal component analysis (PCA) and partial least squares discriminant analysis (PLS-DA) were employed for these analyses. PCA and PLS-DA score plots were generated with 95% confidence intervals. PCA was primarily used to identify potential outliers, while PLS-DA was used for group separation and to identify the most discriminatory lipids.

Cross-validation (CV) was conducted to evaluate model performance, using 5-fold cross-validation due to the limited number of samples per class. Although 5-fold CV may be less robust than the more conventionally used 10-fold, it was considered a reasonable alternative given the sample size constraints. The analysis was applied to the first five components, with model performance assessed using R^2 (goodness of fit), Q^2 (predictive ability), and accuracy, the latter defined as the proportion of correctly classified samples in each fold. A permutation test with 2,000 repeats, using prediction accuracy during training as the test statistic, was performed to assess the statistical significance of the model. Variable importance in projection (VIP) scores were calculated based on the weighted sum of the squared correlations between each variable and the components, reflecting their contribution to class separation.

A heatmap was generated to visualize the overall metabolic variation across the four experimental groups (HHTg 4 M, HHTg 12 M, Wistar 4 M, Wistar 12 M), focusing on the 20 lipids with the most significant differences by one-way ANOVA. Clustered heatmaps for class averages were also created to assess the primary differences between groups. Additionally, a volcano plot was constructed using a fold change threshold of 1.5 and a p-value threshold of 0.05 to identify differential metabolites based on statistical significance and effect size.

Univariate analysis was performed in R software 4.2.1 (R Foundation for Statistical Computing, Vienna, Austria). Individual lipids were analyzed using two-way analysis of variance (2 W-ANOVA) to assess the effects of strain and age on the dependent variables. The model included the main effects of strain and age, as well as their interaction. Tukey's Honest Significant Difference (HSD) *post hoc* test was applied to explore significant interactions. False discovery rate corrections were applied as appropriate.

Results

Basal metabolic parameters

As shown in Table 1, compared to Wistar controls the HHTg strain showed decreased whole body weight but increased weight of visceral adipose tissue, which increased in age in both rat strains. Elevated fasting glucose levels and increased AUC values during OGTT in HHTg rats indicate impaired glucose tolerance, worsening progressively with age. Additionally, the HHTg strain displayed severe dyslipidaemia, characterised not only by significantly elevated genetically determined triglyceride concentrations but also by reduced HDL cholesterol and increased NEFA levels (Fig. 1). In contrast, total serum cholesterol levels were lower in HHTg rats compared to controls but increased significantly with age in both strains (Table 1). No significant differences in adiponectin levels were observed between strains in either serum or muscle; however, adiponectin concentrations declined with age in both groups.

Markers of insulin sensitivity and substrates oxidation in skeletal muscle

Compared to age-matched controls, HHTg animals showed reduced skeletal muscle insulin sensitivity measured as basal and insulin stimulated glycogenesis (Fig. 2). In both strains, skeletal muscle insulin sensitity worsened with age. Decreased skeletal muscle insulin sensitivity in HHTg rats was associated with decreased palmitate oxidation. In contrast, no significant differences in skeletal muscle glucose oxidation were observed between the two strains; however, glucose oxidation declined with age in both strains (Fig. 2).

PKCε and PKCθ in skeletal muscle

No significant differences in relative PKCε protein expression in the cytosolic fraction were observed between the two strains (Fig. 3). However, a reduced relative PKCε protein content was detected in the membrane fraction of 4-month-old HHTg rats compared to age-matched controls. In young HHTg rats, no differences were observed in PKCθ protein expression in either the cytosolic or membrane fractions of skeletal muscle compared with controls. In contrast, significant differences emerged at advanced age, with 12-month-old HHTg rats exhibiting a 78% increase in cytosolic PKCθ protein content and an 87% increase in membrane-associated PKCθ compared to age-matched Wistar controls.

Markers of specific lipids and relative expression of lipid metabolism genes in skeletal muscle

As shown in Fig. 1, the accumulation of both neutral TGs as well lipotoxic DAGs and CERs in skeletal muscle was increased in HHTg rats compared with age-matched controls. Concentration of TGs in muscle was elevated

	W 4 M	HHTg 4 M	W 12 M	HHTg 12 M	P_{strain}	P_{age}
Body weight (g)	407 ± 2	306 ± 5***	622 ± 12	473 ± 9***	<0.001	<0.001
Visceral adipose tissue (mg/g)	2.06 ± 0.11	2.55 ± 0.12	3.22 ± 0.43	5.64 ± 0.14**	<0.001	<0.001
Fasting glucose (mmol/l)	4.8 ± 0.3	5.7 ± 0.2*	5.3 ± 0.3	6.9 ± 0.2***	<0.001	<0.01
Non-fasting glucose (mmol/l)	7.1 ± 0.3	7.6 ± 0.2	6.6 ± 0.1	8.1 ± 0.3	<0.001	n.s.
$AUC_{0\text{-}120}$ (mmol/l)	790 ± 20	907 ± 29*	897 ± 48	978 ± 51	<0.05	<0.05
Insulin (nmol/l)	0.242 ± 0.047	0.335 ± 0.050	0.421 ± 0.062	0.331 ± 0.051*	n.s.	n.s.
Serum TG (mmol/l)	1.57 ± 0.10	5.20 ± 0.31***	1.75 ± 0.10	5.33 ± 0.67***	<0.001	n.s.
Serum cholesterol (mmol/l)	1.76 ± 0.09	1.51 ± 0.05*	2.31 ± 0.12	1.67 ± 0.05***	<0.001	<0.001
HDL-cholesterol (mmol/l)	1.32 ± 0.08	0.59 ± 0.02***	1.55 ± 0.10	0.67 ± 0.01***	<0.001	<0.05
Adiponectin in serum (ng/ml)	5.45 ± 0.31	5.27 ± 0.37	3.85 ± 0.46	3.41 ± 0.31	n.s.	<0.01
Adiponectin in muscle (µg/g)	6.03 ± 0.73	5.86 ± 0.49	4.17 ± 0.51	3.67 ± 0.29	n.s.	<0.01
FGF21 in serum (pg/ml)	112.71 ± 9.46	78.25 ± 6.01**	80.43 ± 8.25	66.01 ± 0.57	<0.01	<0.01
FGF21 in muscle (pg/mg protein)	95.79 ± 16.45	58.04 ± 12.73*	32.21 ± 5.59	18.33 ± 2.64	<0.05	<0.01
Irisin in serum (ng/ml)	66.69 ± 4.34	49.83 ± 1.07**	72.39 ± 5.56	46.19 ± 1.82***	<0.001	n.s.
Irisin in muscle (ng/mg protein)	374.33 ± 34.07	264.38 ± 36.60*	351.35 ± 22.41	221.73 ± 29.98*	<0.01	n.s.

Table 1. Basal metabolic characteristics. Values are given as mean ± SEM; $n = 7$ for each group; Two-way ANOVA results: P-strain denote the signifikance of the strain effect (W vs. HHTg); P-age denotes the signifikance of the age (4 M vs. 12 M). For multiple comparisons, Fisher's LSD *post hoc* test was used. *$p < 0.05$; **$p < 0.01$; ***$p < 0.001$. W-Wistar rats; HHTg – hereditary hypertriglyceridemic rats; AUC – area under curve; FGF21 – fibroblast growth factor 21; TG – triglycerides.

1.8x, total DAGs 1.4x and total CERs 3x in HHTg animals compared to controls. In addition, in DAG lipid class both groups 1,2 DAG as well 1,3 DAG were significantly elevated in muscles in HHTg rats, but higher muscle accumulation was observed in 1,3 DAG group in HHTg rats (Fig. 4). Further, the changes were observed in each ceramides in muscle – CER 18:00 was higher 2.5x, CER 22:00 and CER 24:00 were higher 3x. The concentrations of CER 24:1 were increased the most, which surprisingly did not change with age (Fig. 4). The accumulation of all other CERs and DAGs in muscles increased significantly with age in both strains.

Significant changes in the relative expression of genes involved in lipid metabolism were observed in skeletal muscle of HHTg rats compared to controls. mRNA gene expression of *Scd1*(stearoyl-coenzyme A desaturase) and *Acaca* (acetyl-coenzyme A carboxylase alpha) were significantly decreased in muscles in HHTg animals while mRNA expression of *Degs1* (delta 4-desaturase sphingolipid 1) was elevated (Figs. 4 and 5). Expression levels of other analysed genes encoding enzymes and transcription factors involved in lipid metabolism did not differ between strains. However, the majority of these genes exhibited age-related downregulation in both strains, indicating a general decline in lipid metabolic capacity with ageing (Fig. 5).

Targeted lipidomics in skeletal muscle

The dataset was initially visualized using hierarchical clustering, with a heatmap illustrating the 25 most significantly altered lipids across the four subgroups (Fig. 6A). This analysis, based on average values for each subgroup, revealed substantial differences in lipid profiles between HHTg and Wistar animals. Age exhibited a comparatively minor influence on lipid profiles, as reflected in the clustering patterns: HHTg 4-month-old and 12-month-old animals grouped together, as did Wistar 4-month-old and 12-month-old animals, with no notable interaction between the two age groups.

PCA plot did not reveal distinct clustering patterns, likely due to the relatively subtle changes in lipid profiles. To refine the analysis, supervised PLS-DA modeling was performed to identify lipids that maximized group separation. The resulting PLS-DA model (Fig. 6B) demonstrated a clear distinction between HHTg and Wistar animals, with minimal effects attributable to age, aligning with the unsupervised clustering results. Model validation using 5-fold cross-validation yielded an accuracy of 73%. The optimal model performance required a minimum of five lipids, achieving a strong data fit ($R^2 = 0.82$) and high predictive capacity ($Q^2 = 0.97$) (Fig. 6C). Although the permutation test narrowly failed to reach statistical significance ($p = 0.08$), this may be attributed to the relatively modest dataset size, with more precise validation requiring a larger sample. Nevertheless, the model strongly indicates that strain, rather than age, is the primary determinant of lipidomic differences. Analysis of VIP scores (Fig. 6D) identified phosphatidylethanolamines (PEs) as the most discriminatory lipids,

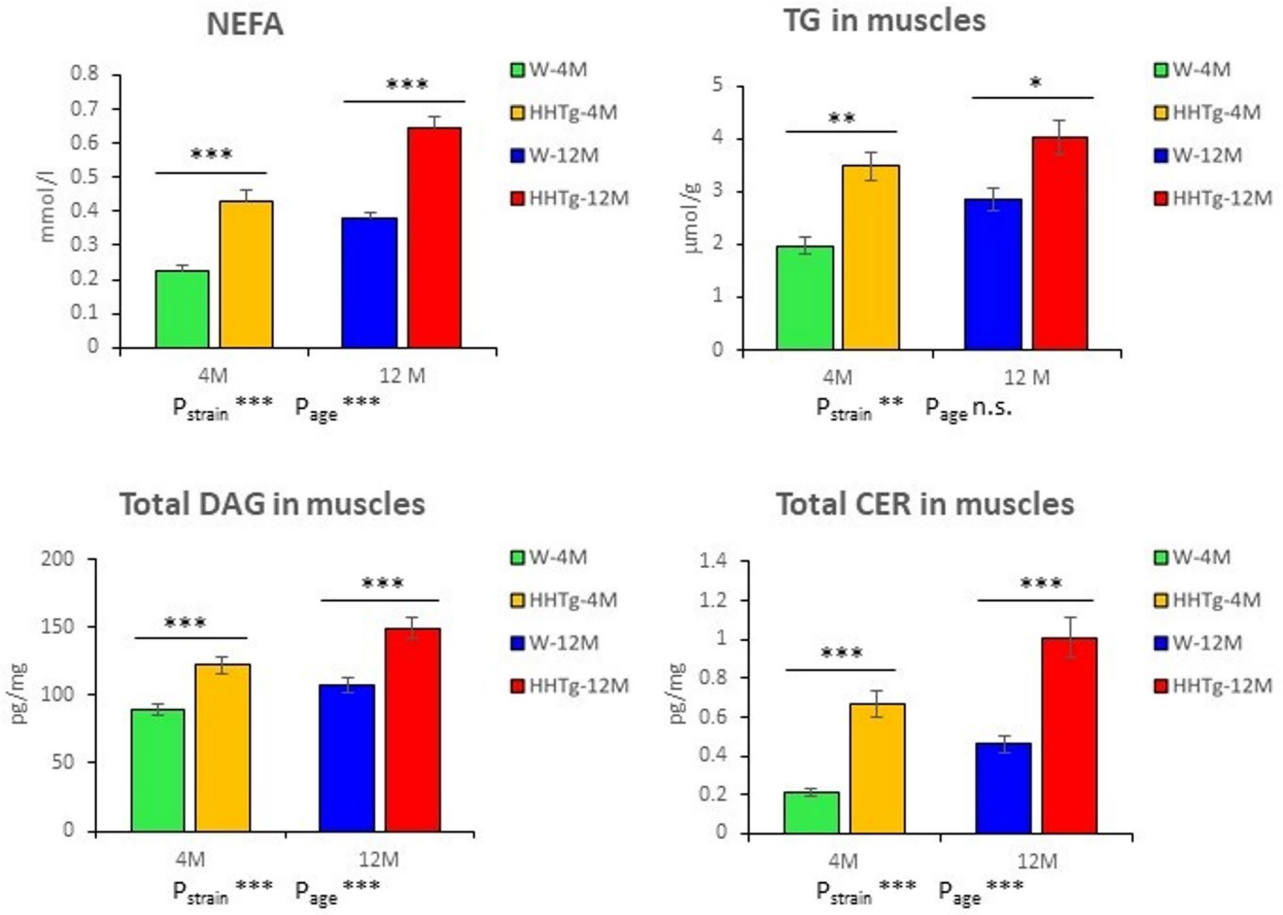

Fig. 1. Serum NEFA, and total TG, DAG and CER in skeletal muscle in Wistar control and prediabetic HHTg rats at 4 and 12 months of age. TG-triglycerides, DAG-diacylglycerols, CER-ceramides. Data are expressed as mean ± SEM and analysed by two-way ANOVA; $n = 7$, * denotes $p < 0.05$, ** denotes $p < 0.01$, *** denotes $p < 0.001$.

with additional contributions from phosphoethanolamine (PE-O) and lysophosphatidylcholines (LPCs), highlighting their potential role in distinguishing between HHTg and Wistar animals.

A total of 336 lipid compounds were detected in skeletal muscle using targeted lipidomic analysis. Two-way ANOVA (Fig. 7; Supplementary Tables 1 and 2) revealed a strong strain effect, with 72 lipids showing significant differences between HHTg and Wistar animals. The most significantly altered lipids were PEs with very long chains (> 39 C), with PE 42:6 (Fig. 7A), PE 39:8, PE 41:2 (Fig. 7B), and PE 43:6 (Fig. 7C) exhibiting the strongest significance (all $p_{strain} < 0.0001$). This suggests substantial alterations in membrane lipid composition. From other lipid classes, the most altered species included PE-Os, primarily PE-O 40:8 (Fig. 7D, $p_{strain} < 0.0001$), PE-O 42:6 (Fig. 7E, $p_{strain} = 0.001$), and PE-O 40:7 (Fig. 7F, $p_{strain} = 0.005$, $p_{age} = 0.002$), all being significantly associated with strain, except for PE-O 40:7 altered both with strain and age. Finally, the most affected lipid classes included PEs, TGs, and DAGs (Supplementary Table 1). The enrichment of PEs, essential components of cellular membranes, suggests potential differences in membrane fluidity and function between the strains. Meanwhile, changes in TG and DAG levels indicate variations in lipid storage and energy metabolism, consistent with altered lipid mobilization pathways in HHTg rats. These findings are further supported by the volcano plot (Fig. 6E), comparing HHTg and Wistar animals irrespective of age, which revealed an increase in certain TGs with very long chains, with TG 56:6 and TG 56:5 (Fig. 6E) being the most significantly elevated.

Age-related effects were also observed, with 32 lipids significantly altered. The most notable was PE-O 40:5 (Fig. 7G, $p_{age} < 0.0001$). Age-related changes primarily affected PEs and CERs, which are associated with membrane integrity and cellular stress responses. Additionally, alterations in LPCs and LCP-Os, such as LPC-O 16:1 (Fig. 7H, $p_{age} = 0.06$) suggest changes in membrane remodeling, potentially reflecting lipid oxidation or inflammatory processes associated with ageing.

Interaction effects between strain and age were less pronounced, with only 12 significant lipids, the most significant being DAG 37:5 (Fig. 7I, $p_{interaction} = 0.004$). The relatively high $p_{interaction}$ for the main affected lipid classes, in terms of both strain and age suggest that while both strain and age independently influence lipid profiles, their combined effect is relatively minor. This indicates that strain differences dominate the lipidomic variation, with age-related changes occurring in a more moderate and independent manner.

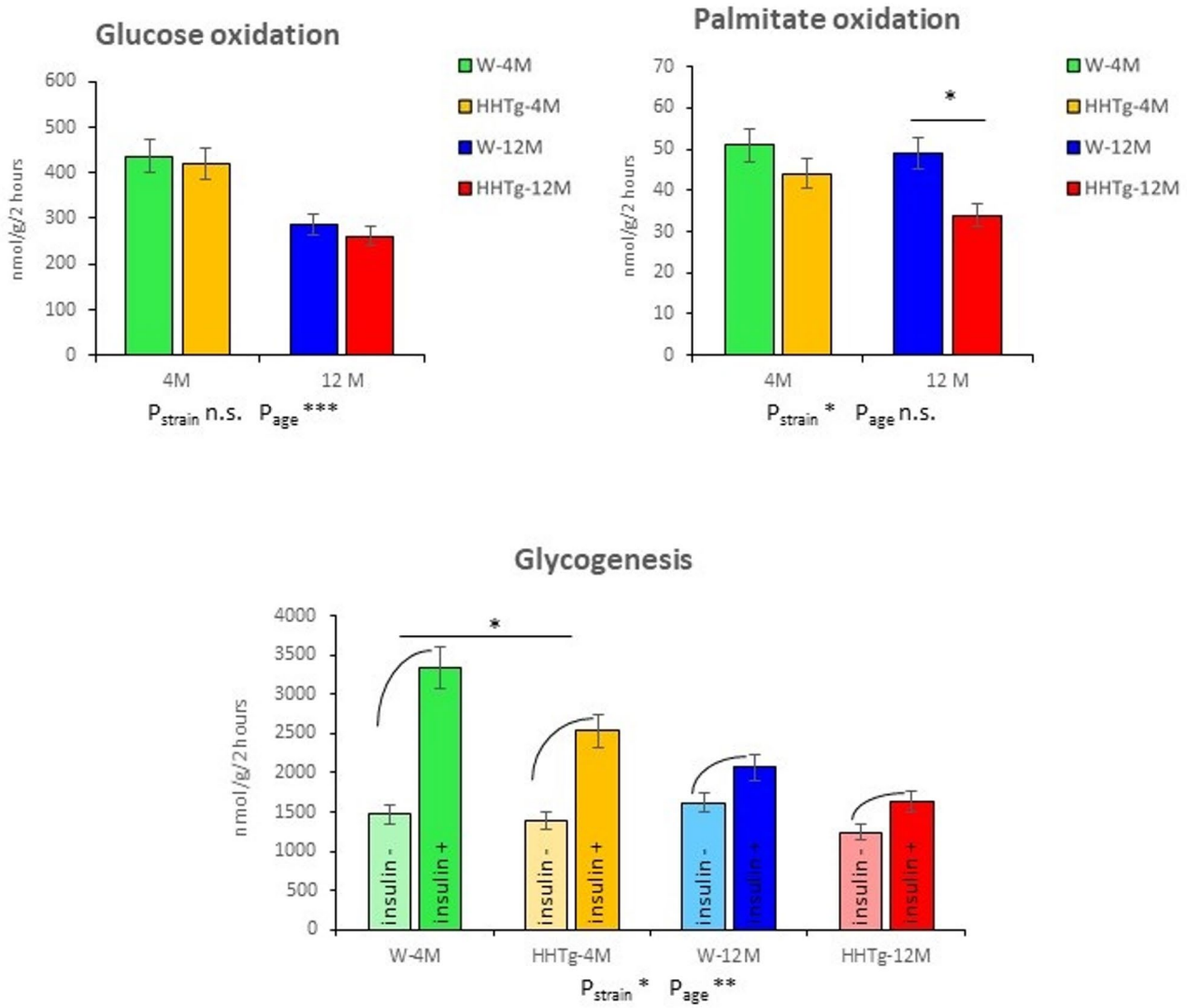

Fig. 2. Glucose and palmitate oxidation, and parameter of insulin sensitivity (glycogenesis) in skeletal muscle in Wistar control and prediabetic HHTg rats at 4 and 12 months of age. Data are expressed as mean ± SEM and analysed by two-way ANOVA; $n = 7$, * denotes p<0.05, ** denotes $p < 0.01$, *** denotes $p < 0.001$.

Correlation analyses (Fig. 8) revealed distinct associations between skeletal muscle lipid species and metabolic parameters in HHTg rats (4-month-old) compared with Wistar controls (4-month-old). In HHTg animals (A), insulin-stimulated and basal glycogenesis negatively correlated with several ceramides (CER 18:0, CER 22:0) and positively with phospholipids and lysophospholipids (LPC 22:6, LPE 20:0, PE 41:2). Non-fasting glucose and impaired fatty acid oxidation also associated with higher ceramide content, while decreased levels of phospholipids showed positive relationships with insulin resistance markers. In contrast, Wistar rats (B) showed a simpler pattern, with largely positive correlations between phospholipids/lysophospholipids and insulin sensitivity indices, and only weak associations with ceramides. The consistency of the observed associations supports a robust link between ceramide accumulation, reduced phospholipids, and impaired muscle insulin action in the HHTg strain.

Discussion

Ectopic lipid accumulation and the generation of lipotoxic intermediates are recognised as key contributors to the development of IR in skeletal muscle. Circulating lipids and their composition play a critical role in promoting ectopic lipid deposition and modulating skeletal muscle insulin sensitivity. In addition to severe hypertriglyceridaemia, the HHTg strain is characterised by chronically elevated serum NEFA levels, which increase with age and have been associated with qualitative alterations in fatty acid (FA) composition within the NEFA lipid class. As reported in our previous study[19], HHTg rats display an increased proportion of saturated FAs and a decreased PUFA-n3 profile. In line with our findings, elevated plasma NEFA levels have been closely associated with increased intramyocellular lipid content and reduced insulin sensitivity in humans[2].

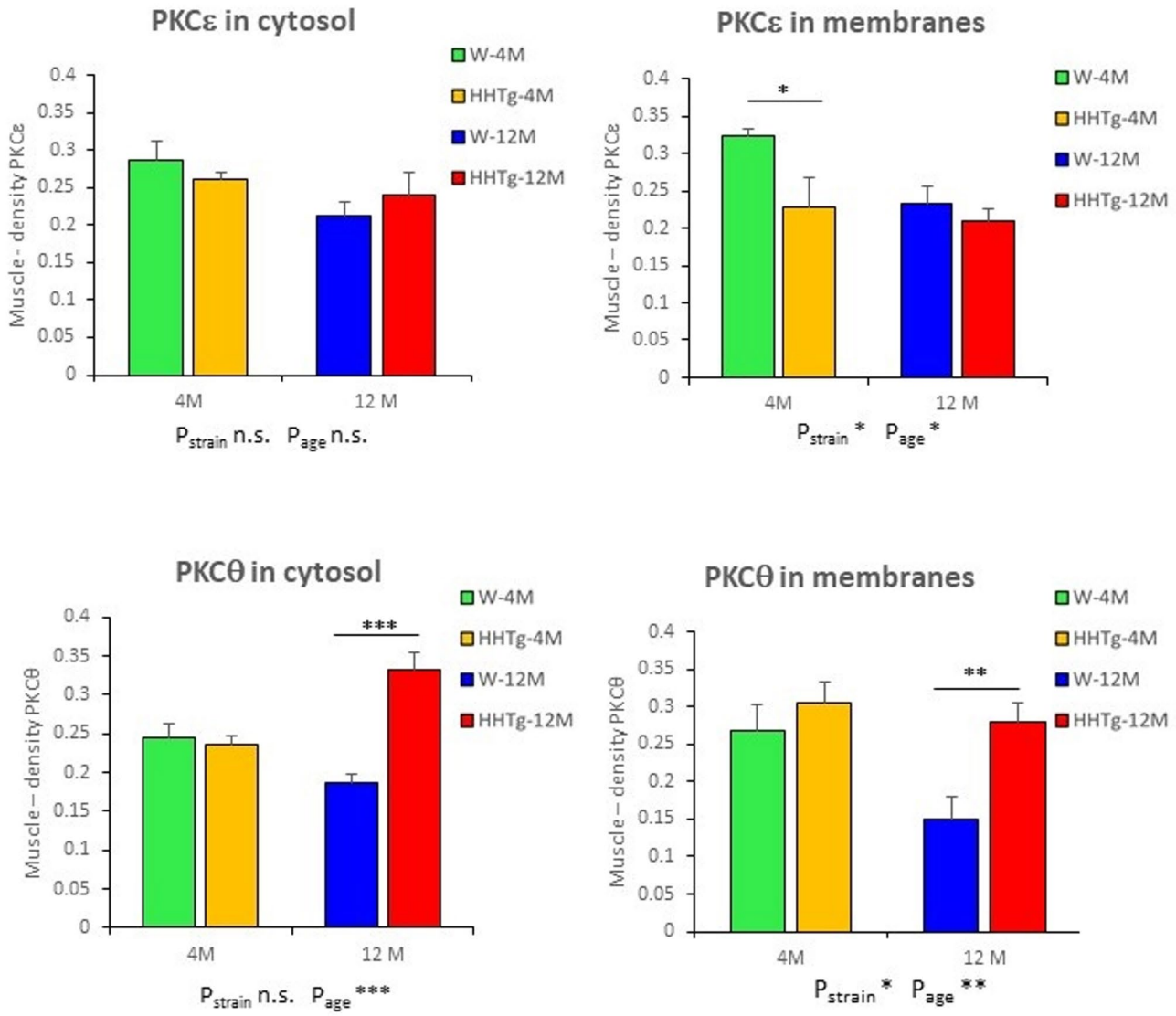

Fig. 3. PKCε and PKCθ in skeletal muscle in Wistar control and prediabetic HHTg rats at 4 and 12 months of age. Data are expressed as mean ± SEM and analysed by two-way ANOVA; $n = 7$, * denotes $p < 0.05$, ** denotes $p < 0.01$, *** denotes $p < 0.001$.

Ectopic lipid deposition in muscle results from either a limited capacity of adipose tissue to accumulate lipids or impaired cellular regulation of lipid storage and utilization. According to human and animal studies, IR is accompanied by ectopic accumulation of neutral TGs in skeletal muscle, but TGs per se may not contribute to IR. TGs as neutral lipids are metabolically inert[20], so lipotoxicity only becomes apparent with the formation of lipotoxic intermediates such as DAGs and CERs generating from them. Interestingly, previous studies have shown that the relationship between IR and skeletal muscle TG content is independent of total adiposity[21], a finding consistent with our observations.

Ectopic lipid accumulation in skeletal muscle disrupts metabolic homeostasis by impairing FA oxidation as well as glucose transport and utilization[22,23]. Reduced *Acaca* gene expression may contribute to the reduced fatty acid oxidation observed in HHTg rats. Our results point out to decreased FA oxidation as an early step in IR development that can precede impaired glucose oxidation in muscle. In particular, ectopic lipids in muscle produce lipotoxic intermediates such as DAGs and CERs that are able to interfere with insulin signaling. Several animal and human studies have implicated DAGs and CERs as major mediators of lipid-induced IR[24,25]. However, the effects of individual lipid species and their composition are also important.

Ectopic DAGs accumulation in muscle may modulate insulin sensitivity through activation of novel protein kinase C (nPKC) isoforms. PKCθ, the predominant nPKC isoform expressed in skeletal muscle, has been frequently implicated in the impairment of insulin action. Accumulated DAGs have been shown to recruit PKCθ to the plasma membrane, leading to its activation, subsequent inhibitory phosphorylation of IRS1 (insulin receptor substrate 1), and disruption of downstream insulin signaling, ultimately resulting in reduced glucose

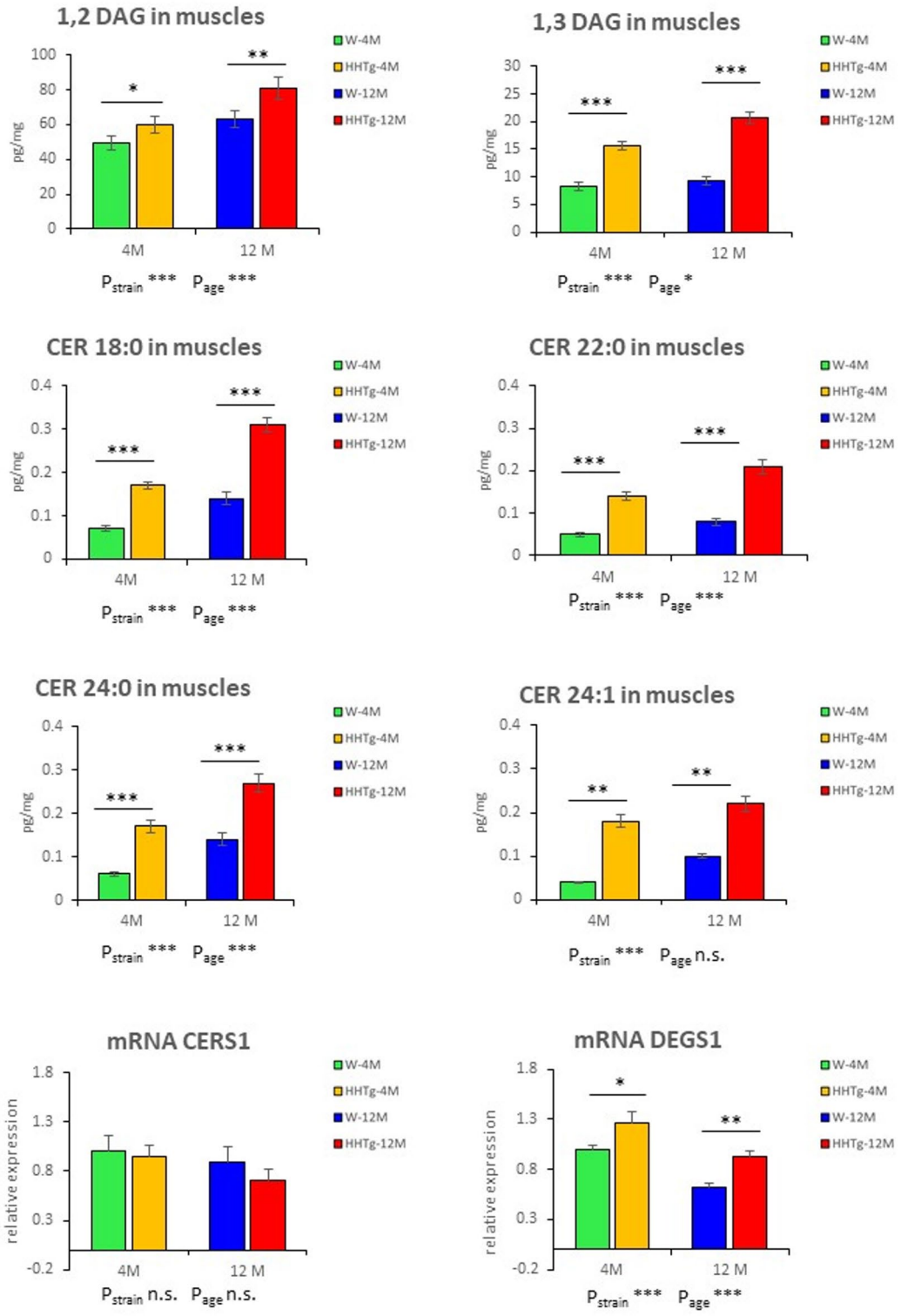

Fig. 4. Lipotoxic DAGs and CERs in skeletal muscle and relative mRNA gene expression of *Cers1* and *Degs1* enzymes in Wistar control and prediabetic HHTg rats at 4 and 12 months of age. CERS1 – ceramide synthase 1, DEGS1 - delta 4-desaturase sphingolipid 1. Data are expressed as mean ± SEM and analysed by two-way ANOVA; $n = 7$, * denotes $p < 0.05$, ** denotes $p < 0.01$, *** denotes $p < 0.001$.

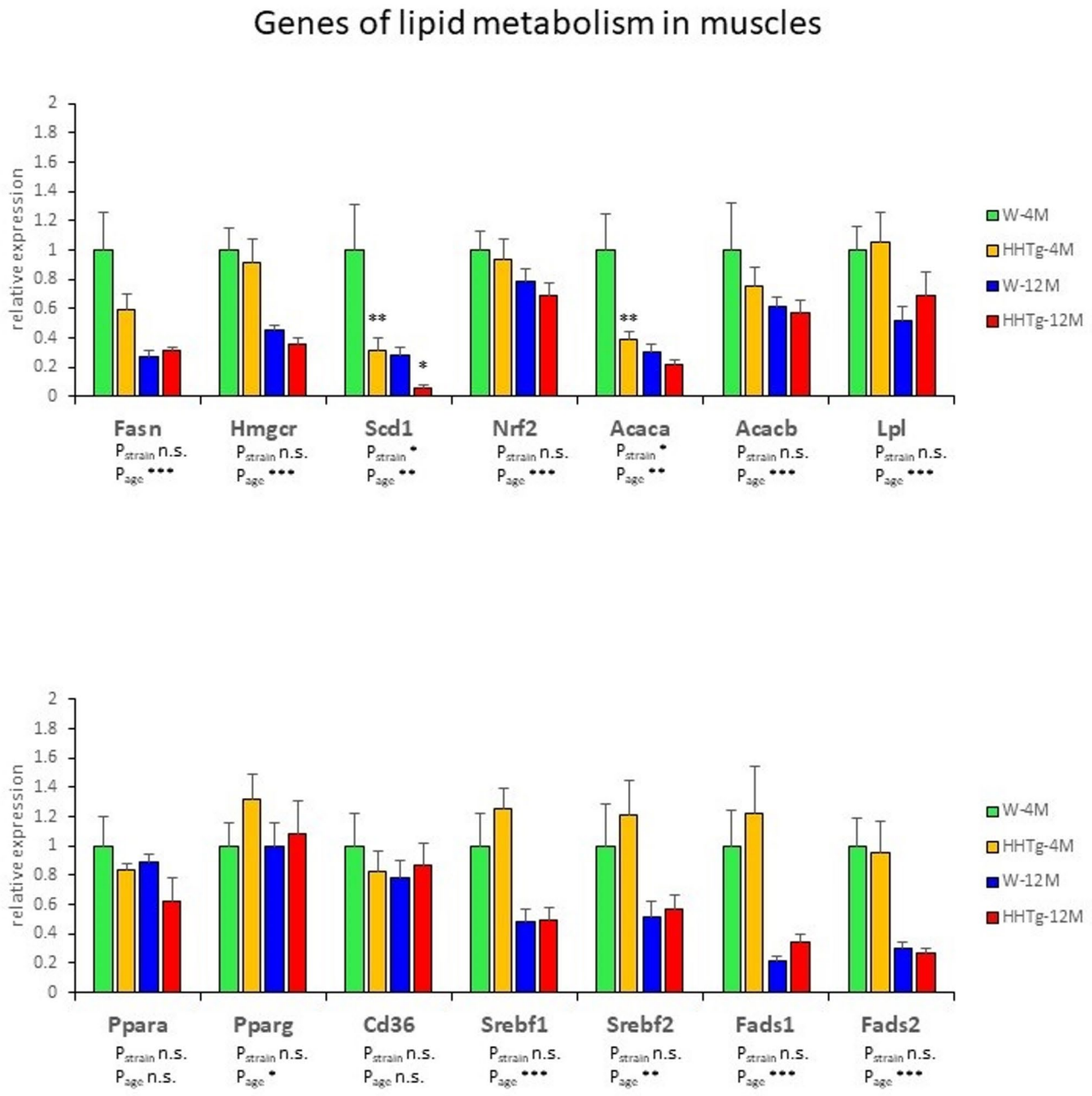

Fig. 5. Relative mRNA gene expression of lipid metabolism enzymes and transcription factors in skeletal muscle in Wistar control and prediabetic HHTg rats at 4 and 12 months of age. Data are expressed as mean ± SEM and analysed by two-way ANOVA; $n = 7$, * denotes $p < 0.05$, ** denotes $p < 0.01$, *** denotes $p < 0.001$.

uptake. Several studies have reported activation of PKCθ or increased PKCθ protein content in the skeletal muscle of insulin-resistant animal models[26–28].

Among DAG isomers, 1,2-DAG has been identified as the only stereoisomer capable of activating nPKCs, and is therefore considered the principal DAG species responsible for the impairment of insulin signaling[29,30]. Although muscle 1,3-DAG concentrations were significantly elevated in HHTg rats compared to age-matched controls, this isomer does not appear to play a major role in nPKC activation. In contrast, PKCθ expression was increased in older HHTg rats, coinciding with a more pronounced accumulation of 1,2-DAG, whereas PKCε levels remained largely unchanged. It is important to note that individual PKC isoforms differ in their expression patterns within skeletal muscle, with expression levels varying during differentiation, and distinct isoforms fulfilling different functional roles. Our findings, highlighting the potential role of 1,2-DAG accumulation and PKCθ activation in the development of IR.

Detailed analysis of skeletal muscle lipids in HHTg rats revealed significantly increased levels of CERs in particular 18:0 and 24:0, alongside increased expression of *Degs1*, a key enzyme in ceramide biosynthesis.

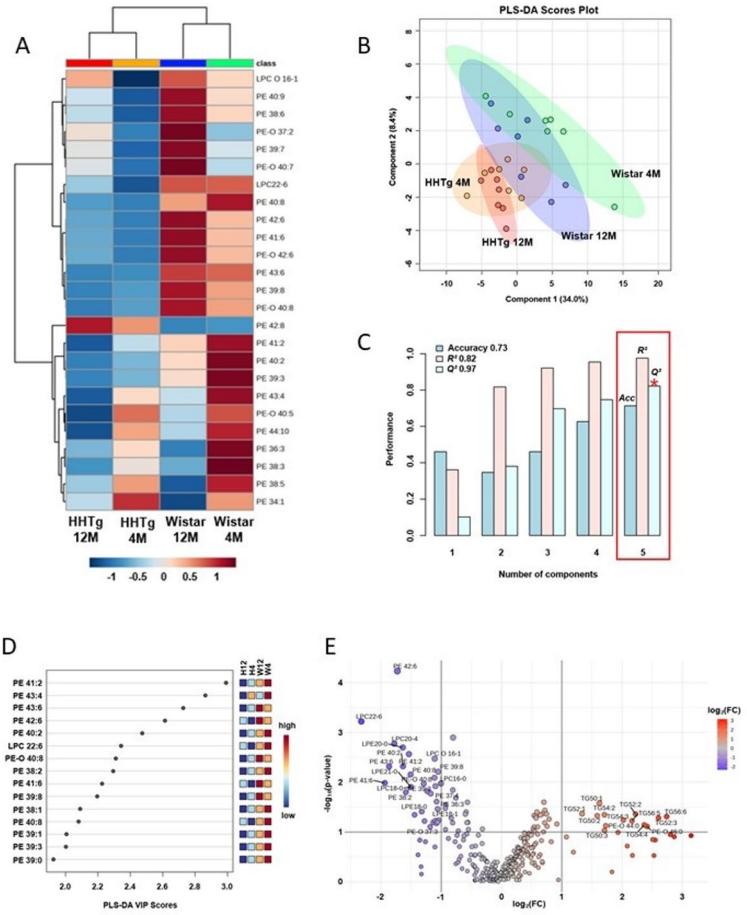

Fig. 6. Skeletal muscle lipidomics in Wistar control and prediabetic HHTg rats. **(A)** Hierarchical clustered heatmap displaying the 25 most significantly altered lipids across the four experimental groups (Wistar 4-month-old, Wistar 12-month-old, HHTg 4-month-old and HHTg 12-month-old). **(B)** Two-dimensional scores plot from partial least squares-discriminant analysis (PLS-DA), illustrating the clustering of the four groups. **(C)** PLS-DA model cross-validation results indicating that a minimum of five components (lipids) is required to achieve optimal predictive performance as determined by the Q^2 value (denoted by *). **(D)** Variable importance in projection (VIP) scores from the PLS-DA model, highlighting phosphatidylethanolamines (PEs) as the primary contributors to group differentiation. **(E)** Volcano plot comparing lipid alterations between all HHTg and all Wistar animals (irrespective of age), showing log2 fold change (FC) of HHTg/Wistar on the x-axis and -log10 raw p-value from an unpaired t-test ($p < 0.05$) on the y-axis. Lipids significantly increased in HHTg animals are marked in red.

Compared to DAGs, the accumulation of CERs was more pronounced, suggesting that skeletal muscle IR in HHTg rats may be more strongly driven by ceramide-mediated mechanisms than by DAGs accumulation. In contrast, DAGs accumulation was more apparent than CERs in skeletal muscle of ZDF animals[31]. In humans, the levels of muscle C18:0, C16:0, C18:1 CERs inversely correlated with insulin sensitivity[32]. According to human lipidomic study[8], CER 18:0 in muscle was the only lipid higher in IR independent of overweight/obesity. In a study using obese fa/fa rats, pharmacological inhibition of CER biosynthesis effectively prevented the onset of IR, uderscoring a causal role for CERs in the early pathogenesis of metabolic dysfunction[33]. Consistent with our findings, the importance of CER species in skeletal muscle IR was published by Bergman study with type 2 diabetic individuals[34].

Unlike DAGs, CERs affect the insulin signaling via the PKB/Akt (protein kinase B) signaling pathway. CERs are involved in the regulation of FA oxidation, their increased accumulation impairs glucose utilization in muscle and can activate inflammation and endoplasmic reticulum stress[35]. Interestingly, the action of CERs promotes lipid uptake and further potentiates TGs accumulation. In addition, the binding of saturated FAs to TLR-4 (toll-like receptor 4) triggers the synthesis and accumulation of CERs through the activation of inflammatory pathways[36].

The biological activity of CERs is influenced by their acyl chain length and degree of FA saturation, which together modulate their impact on signaling pathways. IR is associated with an increase in CERs with saturated FAs, particularly C18:0, which were also identified in this study. Conversely, the IR state itself may contribute to elevated CER levels by promoting inflammation and enhancing the availability of CER precursors.

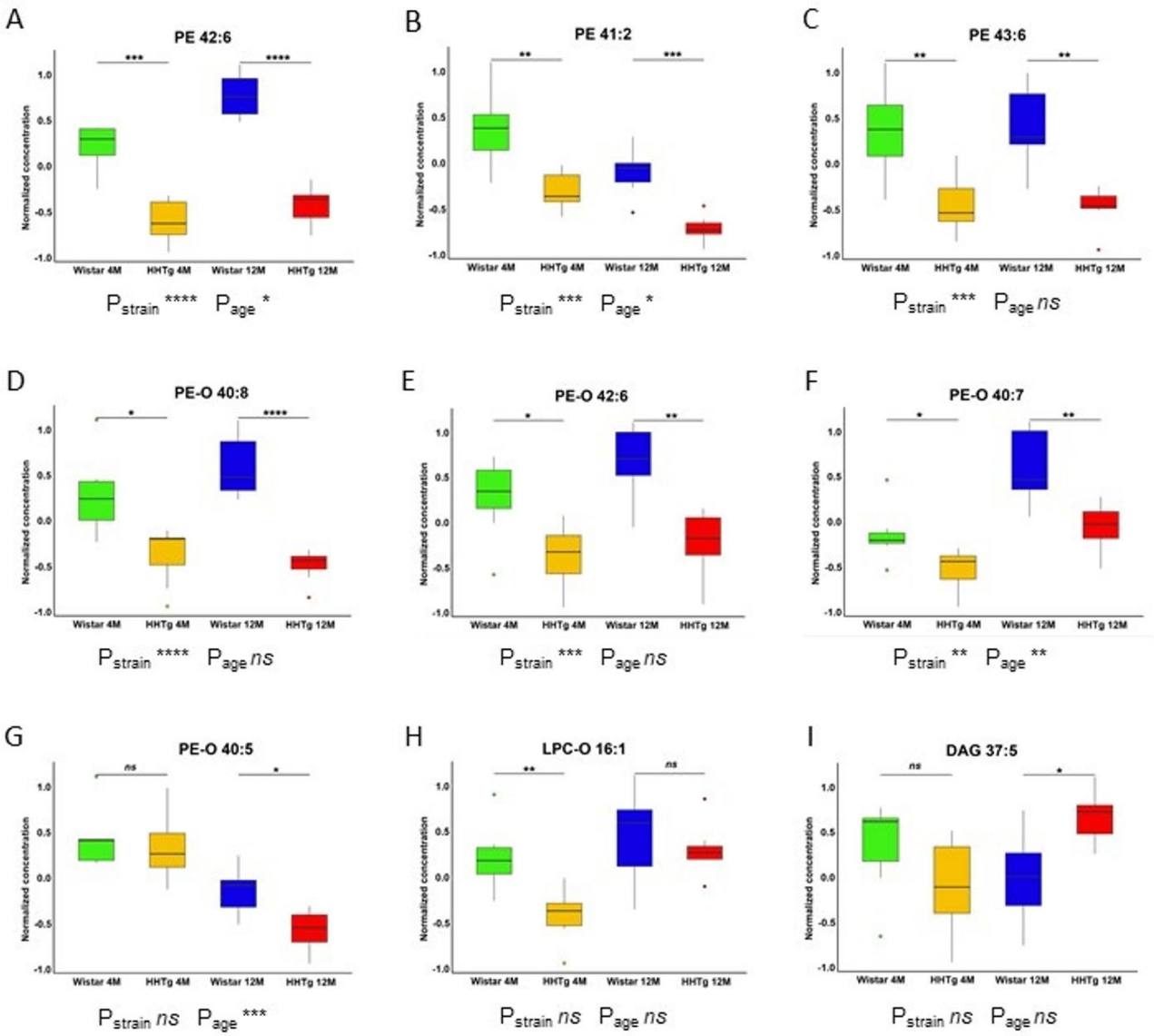

Fig. 7. Two-Way ANOVA and *post hoc* analysis of lipidomic profiles in HHTg and Wistar rats: Two-Way ANOVA results, along with the primary *post hoc* comparisons focusing on the strain effect for HHTg (4-month-old and 12-month-old) and Wistar (4-month-old and 12-month-old) rats. The analysis assesses the effects of strain, age and their interaction on lipidomic profiles. **(A)** PE 42:6. **(B)** PE 41:2. **(C)** PE 43:6. **(D)** PE-O 40:8. **(E)** PE-O 42:6. **(F)** PE-O 40:7. **(G)** PE-O 40:5. **(H)** LPC-O 16:1. **(I)** DAG 37:5.

In mitochondria, CERs lead to reduced electron transport chain activity and increased mitochondrial outer membrane permeability[37], which may be associated with decreased FA oxidation.

CER accumulation may be linked to the reduced levels of FGF21 and irisin observed in the skeletal muscle of HHTg rats, with a more pronounced reduction in FGF21. Both factors function as myokines influencing insulin sensitivity, promote glucose uptake, and regulate FA oxidation[38,39]. In obese mice, FGF21 has been shown to enhance adiponectin secretion while simultaneously reducing CERs accumulation, thereby mediating insulin-sensitizing effect[40]. In contrast, irisin primarily enhances insulin sensitivity by increasing systemic energy expenditure and mediating muscle–adipose tissue crosstalk[41]. Although most studies on irisin have focused on its induction through exercise, its beneficial metabolic effects may also be exerted independently of physical activity. Furthermore, muscle FGF21 is regulated by PKB/Akt[42] and irisin also has been shown to enhance PI3/Akt insulin signaling. It is therefore possible that CERs affect the secretion and actions of myokines such as FGF21 and irisin, thereby further influencing insulin sensitivity in skeletal muscle.

The phospholipids composition might influence insulin sensitivity of muscle as well as whole body glucose tolerance[43]. Especially the content of PUFA-containing phospholipids in muscle is strongly correlated with insulin sensitivity[44]. These studies were among the first to demonstrate that alterations in phospholipid composition can modulate the activity of membrane proteins involved in insulin signaling and energy metabolism.

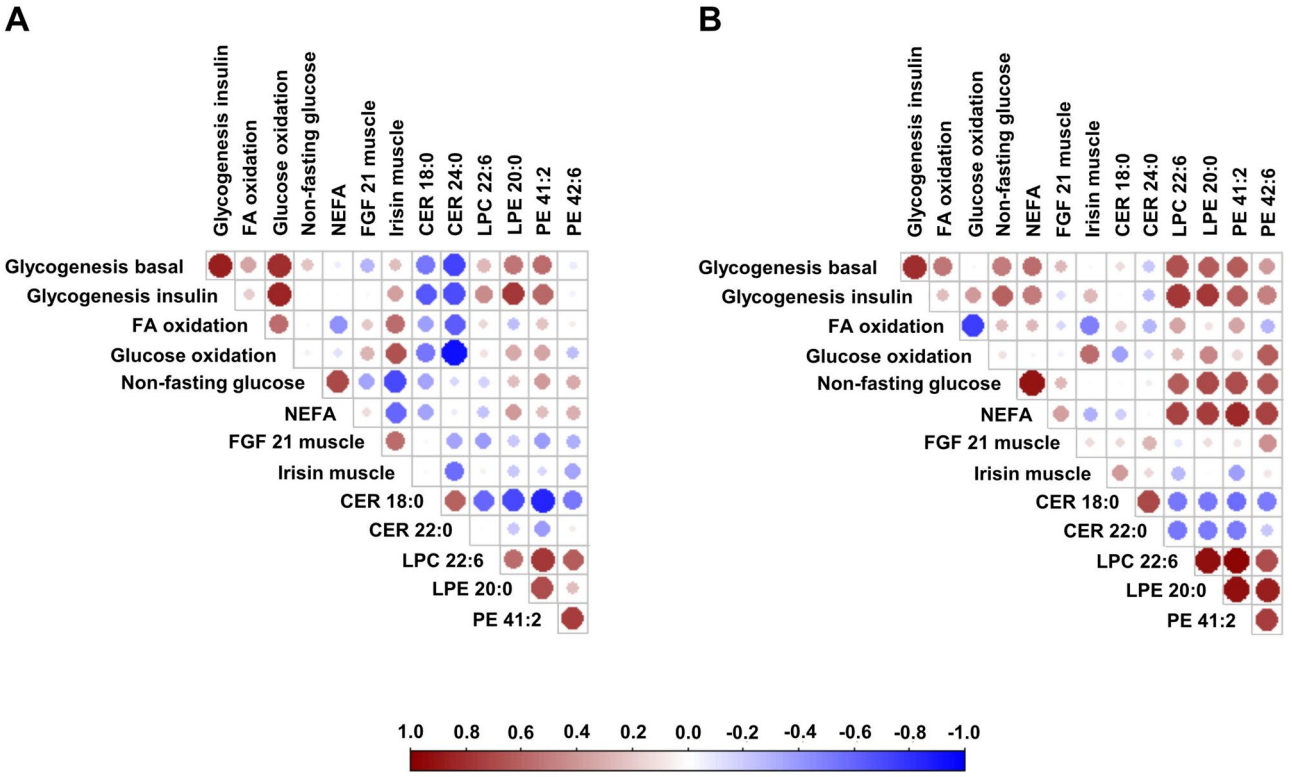

Fig. 8. Correlation plots between skeletal muscle lipid species and metabolic parameters in (A) HHTg 4-month-old rats ($n = 7$) and (B) Wistar 4-month-old controls ($n = 7$). The colour and size of each circle represent the strength and direction of Pearson's correlation coefficient (red = positive, blue = negative).

Based on lipidomic analysis, our study revealed significant changes in specific phospholipids and lysophospholipids in skeletal muscle, in particular some of PEs and PE-O and some of lysophosphatidylethanolamines (LPEs) and LPCs were reduced in association with reduced insulin sensitivity. Interestingly, lipidomic analyses of the HHTg strain revealed minimal differences between young and old animals. These alterations were more pronounced between strains than across age groups, suggesting their involvement in the early stages of muscle IR development. HHTg rats exhibit distinct shifts in PE, TG, and DAG profiles that may be linked to higher lipid turnover or metabolic dysregulation in HHTg rats compared to Wistar, possibly involving altered lipid transport, lipolysis, or insulin sensitivity.

Impaired muscle insulin sensitivity in HHTg strain was associated with decreased phospholipids and lysophospholipids that are important for structual integrity and function of mitochondria, membrane potential and substrate transport[45]. The changes in phospholipids may affect insulin sensitivity due to their role in membrane structure, fluidity, and lipid rafts, affecting various signaling pathways or receptors and metabolic pathways such as glucose uptake or FA oxidation. The physiochemical properties of membranes themselves could predominately drive defective insulin signaling[46].

Based on our lipidomic findings, PEs emerged as the most altered phospholipid class in skeletal muscle in relation to IR. PEs represent a major component of the inner mitochondrial membrane and are critical for maintaining mitochondrial structure and function. Additionally, CERs may compromise mitochondrial integrity by increasing the permeability of the outer mitochondrial membrane. All these alterations can affect multiple mitochondrial function including oxidative phosphorylation, contribute to mitochondrial dysfunction and can lead to reduced FAs oxidation observed in HHTg rats in this study. Subsequently, impaired FA oxidation produces lipotoxic intermediates or atypical lipid metabolites that interefere with insulin and other signaling pathways, thereby exacerbating IR. In addition to mitochondria, changes in phospholipids can affect endoplasmic reticulum membranes. The PC: PE ratio in endoplasmic reticulum membrane is increased in IR muscle cells of humans[47]. Reduced gene expression of enzymes involved in lipid metabolism (*Acaca*, *Scd1*) may contribute to the reduction of PE and other phospholipids and lysophospholipids in HHTg rat strain.

To date, PE in skeletal muscle has been investigated in only a limited number of studies in the context of IR. Lee et al.[48] demonstrated that the PC: PE ratio is inversely correlated with insulin sensitivity in skeletal muscle, suggesting a potential role for membrane phospholipid composition in modulating insulin action. According to a lipidomic study with overweight individuals[8], IR was characterized by higher DAG and lower LPC species in plasma, while in muscle IR was predominantly associated with higher C18:0 sfingolipids. Consistent with our results, this study identified C18:0 CER in muscle as a potencial player in IR independent of excess adiposity, but did not reveal any changes in specific phospholipids or LPC. Currently, there is limited information on the specific roles of individual LPE or LPC species in skeletal muscle; however, evidence from studies in primary

myocytes suggests that increasing LPC may enhance insulin action in muscle tissue[49]. LPCs are likely important components of lipid rafts, and alterations in their composition may impact membrane-associated functions, including signaling pathways mediated by these microdomains.

A limitation of the study is the use of only male rats to maximize homogeneity of the experimental groups. We were unable to assess potential sex-specific differences in skeletal muscle lipidomics. Although changes in mRNA levels of lipid metabolism enzymes provide valuable insights, it should be noted that they do not necessarily reflect enzymatic activities.

Conclusion

Our lipidomic analysis in a prediabetic HHTg rat model reveals that early skeletal muscle insulin resistance may arise independently of obesity and prior to overt diabetes. HHTg strain is characterised by the accumulation of diacylglycerols and, more prominently, ceramides – both known antagonists of insulin signaling – alongside a reduction in specific phospholipids and lysophospholipids. The observed lipid alterations are consistent with impaired fatty acid oxidation and enhanced ceramide biosynthesis, leading to the formation of lipotoxic intermediates. Notably, strain-specific lipid handling and storage pathways exert a greater influence on muscle insulin sensitivity than age-related factors, underscoring a potential metabolic signature of early insulin resistance. These insights highlight the critical role of intramyocellular lipid composition in the pathogenesis of insulin resistance and offer mechanistic targets for early intervention.

Data availability

The data used to support the findings of this study are available from the corresponding author upon request.

Received: 22 August 2025; Accepted: 30 September 2025
Published online: 05 November 2025

References

1. DeFronzo, R. A. & Tripathy, D. Skeletal muscle insulin resistance is the primary defect in type 2 diabetes. *Diabetes Care*. **32** (Suppl 2), S157–S163 (2009).
2. Brechtel, K. et al. Fast elevation of the intramyocellular lipid content in the presence of Circulating free fatty acids and hyperinsulinemia: a dynamic 1H-MRS study. *Magn. Reson. Med.* **45** (2), 179–183 (2001).
3. Leonard, B. L., Watson, R. N., Loomes, K. M., Phillips, A. R. & Cooper, G. J. Insulin resistance in the Zucker diabetic fatty rat: a metabolic characterisation of obese and lean phenotypes. *Acta Diabetol.* **42** (4), 162–170 (2005).
4. Divisova, J., Kazdova, L., Hubova, M. & Meschisvili, E. Relationship between insulin resistance and muscle triglyceride content in Nonobese and obese experimental models of insulin resistance syndrome. *Ann. N Y Acad. Sci.* **967**, 440–445 (2002).
5. Jacob, S. et al. Association of increased intramyocellular lipid content with insulin resistance in lean nondiabetic offspring of type 2 diabetic subjects. *Diabetes* **48** (5), 1113–1119 (1999).
6. Yang, Q., Vijayakumar, A. & Kahn, B. B. Metabolites as regulators of insulin sensitivity and metabolism. *Nat. Rev. Mol. Cell. Biol.* **19** (10), 654–672 (2018).
7. Broskey, N. T., Obanda, D. N., Burton, J. H., Cefalu, W. T. & Ravussin, E. Skeletal muscle ceramides and daily fat oxidation in obesity and diabetes. *Metabolism* **82**, 118 (2018).
8. Tonks, K. T. et al. Skeletal muscle and plasma lipidomic signatures of insulin resistance and overweight/obesity in humans. *Obes. (Silver Spring)*. **24** (4), 908–916 (2016).
9. Preuss, C. et al. A new targeted lipidomics approach reveals lipid droplets in liver, muscle and heart as a repository for Diacylglycerol and ceramide species in Non-Alcoholic fatty liver. *Cells* **8**, 3 (2019).
10. Gautam, J. et al. Characterization of lipid signatures in the plasma and insulin-sensitive tissues of the C57BL/6J mice fed on obesogenic diets. *Biochim. Biophys. Acta Mol. Cell. Biol. Lipids*. **1868** (9), 159348 (2023).
11. Zicha, J. et al. Hereditary hypertriglyceridemic rat: a suitable model of cardiovascular disease and metabolic syndrome? *Physiol. Res.* **55** (Suppl 1), 49–63 (2006).
12. Vrana, A. & Kazdova, L. The hereditary hypertriglyceridemic nonobese rat: an experimental model of human hypertriglyceridemia. *Transplant Proc.* **22** (6), 2579 (1990).
13. Malinska, H., Huttl, M., Oliyarnyk, O., Bratova, M. & Kazdova, L. Conjugated Linoleic acid reduces visceral and ectopic lipid accumulation and insulin resistance in chronic severe hypertriacylglycerolemia. *Nutrition* **31** (7–8), 1045–1051 (2015).
14. Neckar, J. et al. Increased expression and altered subcellular distribution of PKC-delta in chronically hypoxic rat myocardium: involvement in cardioprotection. *Am. J. Physiol. Heart Circ. Physiol.* **288** (4), H1566–H1572 (2005).
15. Markova, I. et al. Long-term Pioglitazone treatment augments insulin sensitivity and PKC-epsilon and PKC-theta activation in skeletal muscles in sucrose fed rats. *Physiol. Res.* **59** (4), 509–516 (2010).
16. Peterson, G. L. A simplification of the protein assay method of Lowry et al. which is more generally applicable. *Anal. Biochem.* **83** (2), 346–356 (1977).
17. Duchoslav, E. & Burton, L. Molecular characterization and quantification of lipids with high resolution accurate mass tandem MS techniques. Biomarkers and omics. AB Sciex Technical Note. 2021;RUO-MKT-02-13720-A (2021).
18. Pang, Z. et al. MetaboAnalyst 5.0: narrowing the gap between Raw spectra and functional insights. *Nucleic Acids Res.* **49** (W1), W388–W96 (2021).
19. Markova, I. et al. The effect of lipotoxicity on renal dysfunction in a Nonobese rat model of metabolic syndrome: A urinary proteomic approach. *J. Diabetes Res.* **2019**, 8712979 (2019).
20. Turner, N., Cooney, G. J., Kraegen, E. W. & Bruce, C. R. Fatty acid metabolism, energy expenditure and insulin resistance in muscle. *J. Endocrinol.* **220** (2), T61–79 (2014).
21. Kelley, D. E. & Goodpaster, B. H. Skeletal muscle triglyceride. An aspect of regional adiposity and insulin resistance. *Diabetes Care*. **24** (5), 933–941 (2001).
22. Roden, M. & Shulman, G. I. The integrative biology of type 2 diabetes. *Nature* **576** (7785), 51–60 (2019).
23. Morino, K., Petersen, K. F. & Shulman, G. I. Molecular mechanisms of insulin resistance in humans and their potential links with mitochondrial dysfunction. *Diabetes* **55** (Suppl 2), S9–S15 (2006).
24. Sokolowska, E. & Blachnio-Zabielska, A. The role of ceramides in insulin resistance. *Front. Endocrinol. (Lausanne)* ;**10**, 577 (2019).
25. Samuel, V. T. & Shulman, G. I. The pathogenesis of insulin resistance: integrating signaling pathways and substrate flux. *J. Clin. Invest.* **126** (1), 12–22 (2016).
26. Bell, K. S. et al. Acute reversal of lipid-induced muscle insulin resistance is associated with rapid alteration in PKC-theta localization. *Am. J. Physiol. Endocrinol. Metab.* **279** (5), E1196–E1201 (2000).

27. Yu, C. et al. Mechanism by which fatty acids inhibit insulin activation of insulin receptor substrate-1 (IRS-1)-associated phosphatidylinositol 3-kinase activity in muscle. *J. Biol. Chem.* **277** (52), 50230–50236 (2002).
28. Kolczynska, K., Loza-Valdes, A., Hawro, I. & Sumara, G. Diacylglycerol-evoked activation of PKC and PKD isoforms in regulation of glucose and lipid metabolism: a review. *Lipids Health Dis.* **19** (1), 113 (2020).
29. Chauhan, V. P., Chauhan, A., Deshmukh, D. S. & Brockerhoff, H. Lipid activators of protein kinase C. *Life Sci.* **47** (12), 981–986 (1990).
30. Petersen, M. C. et al. Effect of weight loss on skeletal muscle bioactive lipids in people with obesity and type 2 diabetes. *Diabetes* **73** (12), 2055–2064 (2024).
31. Takagi, H. et al. Acetyl-CoA carboxylase 2 Inhibition reduces skeletal muscle bioactive lipid content and attenuates progression of type 2 diabetes in Zucker diabetic fatty rats. *Eur. J. Pharmacol.* ;**910**, 174451 (2021).
32. Chung, J. O., Koutsari, C., Blachnio-Zabielska, A. U., Hames, K. C. & Jensen, M. D. Intramyocellular ceramides: subcellular concentrations and fractional de Novo synthesis in postabsorptive humans. *Diabetes* **66** (8), 2082–2091 (2017).
33. Shimabukuro, M. et al. Lipoapoptosis in beta-cells of obese prediabetic fa/fa rats. Role of Serine palmitoyltransferase overexpression. *J. Biol. Chem.* **273** (49), 32487–32490 (1998).
34. Bergman, B. C. et al. Muscle sphingolipids during rest and exercise: a C18:0 signature for insulin resistance in humans. *Diabetologia* **59** (4), 785–798 (2016).
35. Chaurasia, B. et al. Targeting a ceramide double bond improves insulin resistance and hepatic steatosis. *Science* **365** (6451), 386–392 (2019).
36. Holland, W. L. et al. Lipid-induced insulin resistance mediated by the Proinflammatory receptor TLR4 requires saturated fatty acid-induced ceramide biosynthesis in mice. *J. Clin. Invest.* **121** (5), 1858–1870 (2011).
37. Gilbert, M. Role of skeletal muscle lipids in the pathogenesis of insulin resistance of obesity and type 2 diabetes. *J. Diabetes Investig.* **12** (11), 1934–1941 (2021).
38. Chen, Z. et al. The potential function and clinical application of FGF21 in metabolic diseases. *Front. Pharmacol.* **13**, 1089214 (2022).
39. Paoletti, I., Coccurello, R. & Irisin A multifaceted hormone bridging exercise and disease pathophysiology. *Int. J. Mol. Sci.* ;**25**, 24 (2024).
40. Holland, W. L. et al. An FGF21-adiponectin-ceramide axis controls energy expenditure and insulin action in mice. *Cell. Metab.* **17** (5), 790–797 (2013).
41. Pierucci, F., Chirco, A. & Meacci, E. Irisin is target of Sphingosine-1-Phosphate/Sphingosine-1-Phosphate Receptor-Mediated signaling in skeletal muscle cells. *Int. J. Mol. Sci.* **24**, 13 (2023).
42. Izumiya, Y. et al. FGF21 is an Akt-regulated myokine. *FEBS Lett.* **582** (27), 3805–3810 (2008).
43. Vessby, B., Tengblad, S. & Lithell, H. Insulin sensitivity is related to the fatty acid composition of serum lipids and skeletal muscle phospholipids in 70-year-old men. *Diabetologia* **37** (10), 1044–1050 (1994).
44. Storlien, L. H. et al. Influence of dietary fat composition on development of insulin resistance in rats. Relationship to muscle triglyceride and omega-3 fatty acids in muscle phospholipid. *Diabetes* **40** (2), 280–289 (1991).
45. Heden, T. D., Neufer, P. D. & Funai, K. Looking beyond structure: membrane phospholipids of skeletal muscle mitochondria. *Trends Endocrinol. Metab.* **27** (8), 553–562 (2016).
46. Pilon, M. Revisiting the membrane-centric view of diabetes. *Lipids Health Dis.* **15** (1), 167 (2016).
47. Paran, C. W. et al. Reduced efficiency of sarcolipin-dependent respiration in myocytes from humans with severe obesity. *Obes. (Silver Spring).* **23** (7), 1440–1449 (2015).
48. Lee, S. et al. Skeletal muscle phosphatidylcholine and phosphatidylethanolamine respond to exercise and influence insulin sensitivity in men. *Sci. Rep.* **8** (1), 6531 (2018).
49. Ferrara, P. J. et al. Lysophospholipid acylation modulates plasma membrane lipid organization and insulin sensitivity in skeletal muscle. *J. Clin. Invest.* **131**, 8 (2021).

Author contributions

Irena Markova: formal analysis, methodology, conceptualization, data curation, writing – original draft. Martina Hüttl: formal analysis, investigation. Jakub Šťastný: formal analysis, methodology. Iveta Zapletalova: formal analysis. Petr Kačer: methodology, supervision. Vladimír Hönig: review and editing. Tereza Kacerova: formal analysis, data curation, writing – original draft. Hana Malinska: conceptualization, supervision, writing – original draft, writing – review and editing. All authors have read and approved the manuscript for publication.

Funding

This work was supported by the Ministry of Health of the Czech Republic-conceptual development of the research organization (Institute for Clinical and Experimental Medicine-IKEM, IN 00023001), by internal grant of Palacky University in Olomouc IGA_LF_2025_009 and by grants CZ-OPENSCREEN – LM2023052 and EATRIS-CZ – LM2023053.

Competing interests

The authors declare no competing interests.

Ethics approval and consent to participate

All experiments were performed in agreement with the Animal Protection Law of the Czech Republic (359/2012) and the Directive 2010/63EU of the European Parliament and of the Council and were approved by the Ethics Committee of the Institute for Clinical and Experimental Medicine, Prague (Protocol Number: 35/2022).

Additional information

Supplementary Information The online version contains supplementary material available at https://doi.org/10.1038/s41598-025-22745-1.

Correspondence and requests for materials should be addressed to I.M.